Naval Research Laboratory
Washington, DC 20375-5320

NRL/MR/6756--97-7942

Single Pulse Emittance Measurement Technique for Intense Relativistic Electron Beams

J. A. GREGOR

University of Maryland
College Park, MD

R. M. MEGER
J. A. ANTONIADES

Charged Particle Physics Branch
Plasma Physics Division

May 16, 1997

REPORT DOCUMENTATION PAGE

Form Approved
OMB No. 0704-0188

1. AGENCY USE ONLY (*Leave Blank*)	2. REPORT DATE	3. REPORT TYPE AND DATES COVERED
	May 16, 1997	Interim Report

4. TITLE AND SUBTITLE

Single Pulse Emittance Measurement Technique for
Intense Relativistic Electron Beam

5. FUNDING NUMBERS

PE - 61153N11

6. AUTHOR(S)

J.A. Gregor,* R.A. Meger, and J.A. Antoniades

7. PERFORMING ORGANIZATION NAME(S) AND ADDRESS(ES)

Naval Research Laboratory
Washington, DC 20375-5320

8. PERFORMING ORGANIZATION REPORT NUMBER

NRL/MR/6756--97-7945

9. SPONSORING/MONITORING AGENCY NAME(S) AND ADDRESS(ES)

Office of Naval Research
Arlington, VA 22217-5660

10. SPONSORING/MONITORING AGENCY REPORT NUMBER

11. SUPPLEMENTARY NOTES

*University of Maryland
Laboratory for Plasma Research
College Park, MD 20742

12a. DISTRIBUTION/AVAILABILITY STATEMENT

Approved for public release; distribution unlimited.

12b. DISTRIBUTION CODE

13. ABSTRACT (*Maximum 200 words*)

A study of emittance measurements using a slit pinhole type emittance meter is conducted using a 1 MeV, 18 ka electron beam. The beam is passed through titanium foils of varying thickness and the emittance is measured downstream. Two different types of emittance masks are used - one composed of tantalum bars with knife edges and another using cylindrical bars of elkonite. The prototype is used to measure the rms emittance and the projected phase space density of a nominal 1 MeV, 16 ka, 25 ns FWHM electron beam. Data is collected optically using an open shutter camera with polaroid film (time integrated). In addition, time resolved data is presented using a gated optical imaging ccd system on a 5 MeV IREB. This study sets a bound on the measurement accuracy to be expected when using this method of data collection and illustrates the effects of two different mask designs.

14. SUBJECT TERMS

Emittance
Intense relativistic electron beam
Diagnostic

15. NUMBER OF PAGES

28

16. PRICE CODE

17. SECURITY CLASSIFICATION OF REPORT	18. SECURITY CLASSIFICATION OF THIS PAGE	19. SECURITY CLASSIFICATION OF ABSTRACT	20. LIMITATION OF ABSTRACT
UNCLASSIFIED	UNCLASSIFIED	UNCLASSIFIED	UL

NSN 7540-01-280-5500

Standard Form 298 (Rev. 2-89)
Prescribed by ANSI Std 239-18
298-102

CONTENTS

SINGLE PULSE EMITTANCE MEASUREMENT TECHNIQUE FOR INTENSE RELATIVISTIC ELECTRON BEAMS

I. INTRODUCTION

In order to understand the propagation of charged particle beams knowledge of the beam emittance is required. Conventional diagnostics are of the destructive type and rely on some form of mask to divide the beam in question into beamlets.[1] The expansion of these beamlets as a function of position is measured downstream of the mask and this information is used to reconstruct the phase space density function describing the dynamics of the original beam. Using conventional methods a probe is scanned across the image plane downstream from the mask. In order to measure the emittance of a pulsed beam, therefore, many 'shots' are required and the beam must be highly reproducible. In this paper we test a design that allows the entire beam profile to be reconstructed from a single beam pulse. This is accomplished by photographing the Cerenkov emissions from a Teflon foil placed in the image plane.

The device was tested at the Naval Research Lab using the 1 MeV, 16 kA, 25 ns (FWHM) pulsed electron beam produced by Pulserad.[2] This accelerator produces electron beams by field emission from a beam diode driven by a Blumlein type pulse forming line. Analysis techniques were developed for reconstructing the 2-D phase space ellipse of the beam and measuring the rms emittance as well as the emittance for an arbitrary number of particles enclosed assuming a beam with a Maxwellian velocity distribution.

II. DESCRIPTION

The emittance diagnostic developed here is of the slit-pinhole type. It is composed of a Tantalum mask and a Teflon Cherenkov foil.[3] The mask is designed to be range thick[4] for 5 MeV electrons and is held at a fixed but adjustable distance from the foil by four stainless steel rods. The

Manuscript approved April 2, 1997

mask contains five slits (0.5 mm x 25 mm) through which portions of the electron beam may pass (this is referred to as the Venetian Blind Mask design). The mask is mounted in a circular stainless steel plate that is threaded around its periphery so that it may be screwed into the 7 3/4" Aluminum mounting plate. This allows the mask to be oriented at any angle about the beam axis. The distance between the mask and the Cherenkov foil is adjustable to allow for measurement over a wide range of emittance. When in use, the Cherenkov foil will give off visible light at the Cherenkov angle (approximately 48°) that is photographed and digitized for analysis. The surface of the Teflon foil is roughened to increase scattering of the Cherenkov emissions, thus relaxing the requirement that the camera be positioned exactly at the Cherenkov angle.

III. THEORY

The motion of a charged particle may be represented as the position of a point in q-p "phase space" where $q_i=\{x,y,z\}$ and $p_i=\{p_z, p_y, p_z\}$. The evolution of a system of identical particles (a beam) may be represented by the motion of a set of points (one for each particle in the system) in a six-dimensional phase space. This system will have associated with it a probability density function $f(p_1, p_2, p_3, q_1, q_2, q_3)$ describing the probability of finding a particle at any particular point in phase space.

In order to simplify our measurement task, thereby making it tractable, we must make some assumptions concerning the beam and its environment. Since the system Debye length is much longer than the interparticle distance the particles can be considered non-interacting with respect to binary collisions.[5] The absence of external electromagnetics fields ensures that the electric and magnetic fields in the system are conservative. Under these conditions Liouville's theorem states that the density of particles in the system is invariant. Put another way, this means that the volume occupied by a fixed number of particles remains the same. The six dimensional volume enclosing all of the particles in the system will in general change shape, but it's volume will remain constant. We also assume that there are no forces coupling the

motion in one degree of freedom (x, y, or z) with the motion in another, allowing us to separate the transverse motion of a particle into two trajectories, one in each of the two-dimensional phase planes {x,x′}, {y,y′} with Liouville's theorem applying separately to the area of each projection. Each plane then forms a two-dimensional "trace-space", the area of which is conserved. Lastly, we assume the beam is symmetric and Gaussian, making the two transverse directions indistinguishable. We can now describe our beam using a two-dimensional phase space density function $f_2(p_1, q_1)$. If the six-dimensional phase space volume enclosing the particles in this beam is an ellipsoid, its projection onto the two-dimensional phase plane will be an ellipse. This is what we reconstruct with the emittance diagnostic. The area of an ellipse enclosing a specified number of beam particles defines the emittance of the beam.

Since practical beams do not have a sharp boundary the definition of emittance is somewhat ambiguous. For an electron beam at or near thermal equilibrium with a Maxwellian distribution in velocity space and a normal (Gaussian) distribution in real space *no* ellipse can be found that encloses *all* of the beam particles and the emittance must be defined for a certain percentage of beam particles enclosed within the ellipse (%P). Common specifications for %P are 90% ($\varepsilon_{90\%}$) and 63% ($\varepsilon_{63\%}$).

One solution to this dilemma is to define a root-mean-square emittance, given by[6]

$$\varepsilon_{rms} = \sqrt{\langle x^2 \rangle \langle x'^2 \rangle - \langle x \cdot x' \rangle^2} \qquad (1)$$

where the brackets denote an average over the phase space distribution. The rms emittance is bounded for most distributions, even if they have do not have a well defined boundary. Four times ε_{rms} is called the effective emittance. This is the definition used in most of the particle trajectory and beam envelope equations. For the Gaussian distribution considered here ε_{eff} will encompass approximately 90% of the particles in the beam.[5] These two definitions of emittance do not relate to one another in a simple way and any relationship between them will vary depending on the beam profile and the nature of external forces on the system.

In order to calculate the spacing between the mask and the Cerenkov foil required for the expected range of beam emittance we must solve the beam envelope equation. The general envelope equation taking into account both emittance and space charge effects is given by,

$$r_m'' - \frac{\varepsilon^2}{r_m^3} - \frac{K}{r_m} = 0 \qquad (2)\ (a)$$

where,

$$K = \frac{2I}{I_o \beta^3 \gamma^3} \qquad I_o = \frac{4\pi\varepsilon_o mc^3}{e} \cong 17\ \text{kA} \qquad (2)\ (b)$$

K is called the generalized perveance (a measure of the collective effect of space charge forces on the beam) and I_0 is the characteristic (Alfvén) current.

The beam radius can be determined numerically at any z position given the generalized perveance, emittance, and initial conditions. Integrating Eq. 2 (a) with $r_m = r_o$ and $r_m' = r_o'$ at z=0 we get

$$z = \int_{r_o}^{r_m} \left[r_o'^2 + \varepsilon^2 \left(\frac{1}{r_o^2} - \frac{1}{r_m^2} \right) + 2K \ln\left(\frac{r_m}{r_o} \right) \right]^{-1/2} dr_m \qquad (3)$$

where K > 0 for an electron beam.

This equation may be solved numerically to determine the expansion of the sheet beamlets as they travel from the mask to the Cherenkov foil, given the beamlet current and expected emittance.[7] For the current density and slit width used in this experiment, the effects of space charge forces were found to be negligible when measuring beams with any significant value of emittance. In this case K = 0 and Eq. (3) becomes, upon integration

$$r_m^2 = r_o^2 - 2 r_o r_o' z + \left[r_o'^2 + \left(\frac{\varepsilon}{r_o} \right)^2 \right] z^2 .$$

IV. EMITTANCE ANALYSIS TECHNIQUE

The analysis technique developed here is applicable to the measurement of a centered symmetric electron beam with a Maxwellian velocity distribution and a Gaussian spacial profile. The technique is a variation of the slit-pinhole method. Regularly spaced slits in a mask fix the x position $x_i = \{x_{-2}, x_{-1}, x_0, x_1, x_2\}$ of the beamlets. A pinhole maps out the position and width, σ_i, of each beamlet. At a given $x=x_i$, fixed by the slit, the width of the corresponding beamlet relates to the length of a vertical cut through the emittance ellipse at that position. The displacement of the beamlet peak relative to the slit centroid $(x_{is} - x_{ip})$ corresponds to the position of the ellipse major axis at x_i. This information is sufficient to reconstruct the position and orientation of the $x - x'$ phase space ellipse (see Fig. 3).

Before placing the emittance diagnostic in the beam line, Eq. (3) is solved to determine the optimum mask to Cherenkov foil distance L required to cover the expected range of emittance. If L is too small the beamlets will be very narrow and an accurate measurement will be difficult. If they are too far apart the beamlets will blend together, complicating the Gaussian fit. Once the mask-foil spacing is set, the diagnostic is placed at the beam line in an evacuated drift tube that contains a window on the Cherenkov foil.

An open shutter photograph is taken of the Cherenkov emissions. The photograph is digitized at 300 dpi using a 256 gray scale scanner and a lineout is taken. The lineout is a plot of image brightness vs x position (across the slits), taken at the y position that corresponds to a cut through the center of the beam. This gives data similar to that derived by scanning a pinhole across the slits at the plane of the Cherenkov foil. It has the advantage of collecting all the information needed to construct an emittance ellipse in a single beam pulse. A conversion from the number of pixels in the digitized image to physical distance (at the Cherenkov foil) is found by digitizing photographs of a scale taped to the foil prior to firing the accelerator.

Custom code was written to fit a five peak Gaussian to the lineout data. The resultant parameters give the position, width, and amplitude of the individual beamlets. A single Gaussian is then fit to the five individual

peaks. This fit represents the incident beam and gives us information on beam radius and centering. The assumption here is that the slits are infinitesimally thin. A finite slit width would increase the actual width of the beamlets measured at the Cherenkov foil. Rhee and Schneider[8] have developed a mathematical technique, applicable to a beam with a Maxwellian transverse velocity distribution, can be applied to correct for this effect. In this experiment the variation due to a finite slit width was below experimental resolution.

Three quantities (data points) are calculated from each beamlet, α_i, β_i, and σ_i. α_i is the angle between two rays emanating from the slit centroid, one extending to the Cherenkov foil parallel to the axis of propagation, the other extending to the beamlet peak (see Fig. 3). It is given by the following relation,

$$\alpha_i = \text{atan}\left((x_p - x_i)/L\right) \tag{4}$$

where x_p is the x position of the corresponding beamlet peak and x_i is the x position of the corresponding slit.

σ_i is the angle between two rays emanating from the slit centroid, one extending to the beamlet peak and the other extending to a point on the beamlet a specified amount down from the peak,

$$\sigma_i = \text{atan}\left((x_p - x_i)/L\right) \tag{5}$$

where x_t is the x position of the desired emittance threshold.

β_i is the peak amplitude of the beamlet emanating from the slit at x_i. Each beamlet gives us one data point for each of the three quantities. These data points can be used to generate smooth curves for three functions. The resultant functions, $\alpha(x)$, $\beta(x)$, and $\sigma(x)$, for a typical Pulserad shot are shown in Figs. 4 and 5. The circles represent the actual data points, α_i, β_i, and σ_i, used to generate the functions.

In order to specify the %P (percentage of particles enclosed) for our emittance measurement we need a relation specifying the number of particles enclosed in the distribution as a function of beam radius. For a

Gaussian particle density function the percentage of particles enclosed within a distance x_t of the peak is given by

$$\%P = \frac{\int_0^{x_t} 2\pi r e^{-r^2/2\sigma^2} dr}{\int_0^{\infty} 2\pi r e^{-r^2/2\sigma^2} dr} = 1 - e^{-x_t^2/2\sigma^2} \tag{6}$$

The distance from the beam peak to a point on the beam corresponding to a given %P is given by,

$$x_t = \sigma\sqrt{-2\ln(1-\%P)} \tag{7}$$

This is the effective radius of the beam. Assuming a Maxwellian profile in velocity space gives us a similar relation for the effective σ_i of each beamlet,

$$\sigma_{eff} = \text{atan}\left(\frac{x_t'}{L}\right) = \text{atan}\left(\frac{\sigma\sqrt{-2\ln(1-\%P)}}{L}\right) \tag{8}$$

With this information an emittance ellipse can be constructed. A simple spreadsheet program was sufficient to conduct a first order analysis.[9] For each slit position x_i, two points on the perimeter of the ellipse are specified. These are given by α_i plus and minus σ_{eff} for the beamlet produced by the slit at x_i. The extent of the ellipse in x is set by the effective radius. To facilitate curve fitting, the data points for the ellipse perimeter can be rotated so that the ellipse major axis coincides with the x axis. The upper half of an ellipsoid can then be fit to the data in the upper half plane using the following relation,

$$y = b\sqrt{\left|1 - x^2/a^2\right|} \tag{9}$$

The area of the ellipse thus constructed corresponds to the emittance of the beam for the specified %P.

Using the curves derived before can also calculate the rms emittance, the two dimensional phase space density function $\rho_2(x,x')$, and

a number N that relates to the total number of particles in the beam by a constant dependent on the characteristics of the Cherenkov foil and the data collection system (camera, film, etc.). The integrals giving $\rho_2(x,x')$, N, and the second moments of the distribution are given by,[10]

$$\rho_2(x,x') = 2\int_x^{\infty} \frac{\beta(r)\exp\left[-(x'-\alpha x/r)^2/2\sigma^2\right]}{\sqrt{r^2-x^2}} r\,dr \qquad (10)(a)$$

$$\langle x'^2 \rangle = \frac{4\sqrt{2\pi}}{N}\int_0^{\infty} x^2 \int_x^{\infty} \frac{\beta\sigma\,dr}{r\sqrt{r^2-x^2}}\,dx \qquad (10)(b)$$

$$\langle x'^2 \rangle = \frac{4\sqrt{2\pi}}{N}\int_0^{\infty}\left[\int_x^{\infty} \frac{\beta\sigma^3 r\,dr}{\sqrt{r^2-x^2}} + \int_x^{\infty} \frac{\alpha^2\beta\sigma\,dr}{r\sqrt{r^2-x^2}}\right]dx \qquad (10)(c)$$

$$\langle xx' \rangle = \frac{4\sqrt{2\pi}}{N}\int_0^{\infty} x^2 \int_x^{\infty} \frac{\alpha\beta\sigma\,dr}{\sqrt{r^2-x^2}}\,dx \qquad (10)(d)$$

$$N = 4\sqrt{2\pi}\int_0^{\infty}\int_x^{\infty} \frac{\beta\sigma r\,dr}{\sqrt{r^2-x^2}}\,dx \qquad (10)(e)$$

V. EXPERIMENTAL RESULTS

All emittance data was recorded using a bellows camera in open shutter mode with a Geromac 1:6.8 f=220mm lens and Type 53 or 57 Polaroid film. The emittance diagnostic was set up inside an evacuated 8" drift tube approximately 2 cm from the anode (exit) foil of the beam diode. The drift tube had arms extending from the sides at the Cherenkov angle as illustrated in Fig. 6. These arms are terminated in glass windows to allow an unobstructed view of the Cherenkov foil. The

distance from the camera lens to the Cherenkov foil was approximately 24 inches.

A spherical cathode tip was used for all shots, and a 1.5 mil titanium exit foil served as the anode of the accelerator diode. In addition, an extra thickness of titanium foil was positioned approximately 1.25 mm prior to the mask. This provided a method for changing the emittance of the beam going into the diagnostic. It also served to block any light caused by the occasional vaporization of the exit foil. When allowed to shine through the venetian mask this light would wash out the desired Cherenkov emissions on the photograph. Scattering in the titanium foil "heats up" the beam, causing an increase in $\Delta\theta$ given by the formula,[11]

$$\Delta\theta = \frac{\sqrt{t}}{\gamma} \tag{11}$$

where t is the thickness of titanium in mils. A γ of 3.15 is used in Eq. (11) based on energy analyzer measurements of the beam.

Photographs of the Cherenkov emissions were digitized and processed as outlined in the previous section. Since the photographs were taken open shutter we are actually measuring a time integrated emittance. The time integrated emittance ellipse will be a summation of 'differential' ellipses weighted by the number of particles present during each 'differential' of time, and will appear fatter than an ellipse measured at any instant in time. The result will be dominated by the emittance prevailing during the majority of the beam length, but will be higher if the ellipse has a different orientation (and significant current density) at various z positions in the beam.

Six shots were taken using Pulserad and analyzed. The emittance was evaluated using a commercial spreadsheet program. The rms emittance and phase-space density function $\rho_2(x,x')$ were evaluated using a custom 'C' program based on the discussion in the previous section. The results of these measurements are tabulated below.

Shot #	Ti (mils)	Beam Radius (mm)	Estimated ε_{eff} (mm-rad)	ε_{eff} Limited (mm-rad)	ε_{eff} Total (mm-rad)	Estimated $\Delta\theta_{eff}$ (rad)	$\Delta\theta_{eff}$ Limited (rad)	$\Delta\theta_{eff}$ Total (rad)
294	2.5	12.75	6.38	5.36	13.96	.50	.33	.66
319	2.5	13.53	6.77	4.48	14.08	.50	.21	.57
320	2.5	12.44	6.22	5.64	11.24	.50	.24	.42
321	2.5	11.76	5.88	5.44	8.40	.50	.23	.31
300	11.5	16.83	18.18	9.12	65.32	1.08	.45	2.16
302	21.5	21.12	31.18	11.88	165.04	1.47	.52	4.55

Table 1 Results of Pulserad emittance analysis for limited and total effective emittance.

Shot #	Ti (mils)	Beam Radius (mm)	Estimated $\varepsilon_{63\%}$ (mm-rad)	$\varepsilon_{63\%}$ (mm-rad)	Estimated $\Delta\theta_{63\%}$ (rad)	$\Delta\theta_{63\%}$ (rad)
294	2.5	18.02	9.05	15.22	.50	.84
319	2.5	19.13	9.61	12.56	.50	.66
320	2.5	17.60	8.83	15.34	.50	.87
321	2.5	16.63	8.35	14.54	.50	.87
300	11.5	23.80	25.62	31.46	1.08	1.32
302	21.5	29.86	43.96	47.17	1.47	1.58

(a)

Shot #	Ti (mils)	Beam Radius (mm)	Estimated $\varepsilon_{90\%}$ (mm-rad)	$\varepsilon_{90\%}$ (mm-rad)	Estimated $\Delta\theta_{90\%}$ (rad)	$\Delta\theta_{90\%}$ (rad)
294	2.5	27.35	13.73	33.12	.50	1.21
319	2.5	29.04	12.18	26.88	.50	.93
320	2.5	26.70	13.40	32.32	.50	1.21
321	2.5	25.24	12.67	31.85	.50	1.26
300	11.5	36.11	38.87	60.22	1.08	1.67
302	21.5	45.32	66.71	92.50	1.47	2.04

(b)

Table 2 Results of Pulserad emittance analysis for (a) 63% and (b) 90% of the particles enclosed.

The Titanium foils used vary in total thickness from 2.5 mils to 21.5 mils and effect emittance through a change in electron transverse velocity due to scattering. To compare theory with experiment we normalize the emittance by the beam radius in order to arrive at an emittance angle $\Delta\theta$. In each table the beam radius, r_m, is derived from the beam s found during the original Gaussian curve fit. For effective emittance $r_m = s$. For $\varepsilon_{63\%}$ and $\varepsilon_{90\%}$ r_m is related to σ by Eq. (7). $\Delta\theta_{63\%}$ and $\Delta\theta_{90\%}$ are found by dividing $\varepsilon_{63\%}$ or $\varepsilon_{90\%}$ by the appropriate beam radius. For the effective emittance, $\Delta\theta_{eff} = \sqrt{2\langle x'^2\rangle} = \overline{x}_{eff}$, from the second moment of the averaged divergence angle of the beam. In all cases the estimated ε is found by multiplying the estimated $\Delta\theta$ (found from Eq. (11)) by the beam radius. Two calculations have been done for effective emittance, total and limited, based on how we handle the projection of $\alpha(x)$, $\beta(x)$, and $\sigma(x)$ outside the know data range.

Plots comparing the measured vs estimated $\Delta\theta$ for this experiment are shown in Figs. 8 through 10.

The solid line in Figs. 3.13 through 3.15 signifies a 1:1 correlation. It can be seen that $\varepsilon_{63\%}$ tracks with the estimated emittance. The fact that the measured emittance is always above the estimated emittance could be indicative an intrinsic beam emittance due to the source or it could be caused by the time integrated nature of the data.

The relationship between effective emittance and the estimated emittance is more problematic. ε_{eff}-limited gives consistently low readings of emittance (unphysical) and does not seem to be well correlated with estimated emittance. ε_{eff}-total is somewhat better. At low emittances ε_{eff}-total is in agreement with the estimate. As emittance is increased the measured value diverges from the estimate. There are two possible explanations for this behavior.

The first lies in the nature of the emittance estimate. Eq. (11) becomes increasingly invalid as foil thickness is increased. When the thickness of the foil becomes a significant fraction of range thickness scattering angles will become very large and the analysis by which Eq. (11) was derived breaks down. In general, scattering angles will be significantly larger than predicted.

The second involves the method by which $\sigma(x)$ and $\alpha(x)$ are reconstructed in the rms emittance analysis. The form of these functions

is, in general, unknown. Within the limits of the available data they can be estimated using a cubic spline interpolation. Outside the radius of the outer slits we can only make a guess as to their form. Analysis using an assumed form for $\sigma(x)$ and $\alpha(x)$ outside the range of available data is yields a 'total' effective emittance. If the assumed form is wrong measurements of effective emittance will be in error. To avoid this we can try setting $\sigma(x)$ and $\alpha(x)$ zero outside the range of available data, yielding a 'limited' effective emittance. Examination of Fig. 9 indicates that some assumption about the behavior of these functions in the wings of the distribution is required to obtain a valid measurement of estimated (or rms) emittance.

Note that in Fig. 10 we have measured emittance angles greater that 90°. This is possible because what we are measuring is the centroid of a Gaussian distribution. Even if the majority of the particles are deflected through > 90° there will be those in one wing of the distribution that are deflected by less and these can be used to reconstruct the entire profile. The reconstruction will not be very accurate but it is possible given a large enough beam current in the wings.

Using Eq. (10)(a) we can construct a phase space density plot for the measured beam. The resultant plot is a family of emittance ellipses. Fig. 11 shows this plot for a typical Pulserad beam.

VI. ERROR ANALYSIS

The major sources of error were examined to determine the impact on device accuracy. Numerical calculations for the device used in this experiment are included to give a feel for the numbers. The sources of error considered include errors due to:

1. Digitization Error - The conversion from pixels on the digitized image to physical distance was derived by digitizing photographs of a scale taped to the Cherenkov foil. Error bars were placed on the digitized data by re-running the emittance analysis with Gaussian fit parameters plus and minus 1/2 pixel from the measured values. This gives an estimate of the error due to the

digitization process. The results are shown in Figs. 11 through 3.20. The error bars for $\beta(x)$ due to digitization error are related to the number of gray levels the digitizer is capable of distinguishing. In this case the error is $.5/255 \cong .2\%$, indistinguishable on a graph.

2. Finite Slit Width - The error due to finite slit width was found to be below experimental resolution.

3. Space Charge Expansion - For the range of emittances seen in this experiment space charge forces are negligible. Since the perveance term in Eq. (2)(b) goes as γ^{-3}, the error due to space charge expansion becomes small for highly relativistic beams. For extremely low emittance beams, however, the increase in measured emittance may be significant.

4. Film Exposure/Focusing - Provided the film is operated within a linear response range as in the present experiments, exposure should not have much effect on emittance measurements. However, if the film is over or under exposed the measured Gaussian fit to the beamlets would give a larger or smaller σ_i than is actually the case. An out of focus image will also result in a larger σ_i. Note that if the camera is focused on the center of the Cherenkov foil the outer beamlets may be slightly out of focus, increasing the value of $\alpha(x)$ in the wings of the curve, and hence increasing the emittance measured.

5. Limited Number of Slits - A more accurate reconstruction of the beam parameters $\alpha(x)$, $\beta(x)$, and $\sigma(x)$ could be made if the number of slits were increased. Comparison of ε_{rms}-limited vs ε_{rms}-total shows that large errors are introduced if the parameters are assumed zero outside the known data range. Even a guess will improve the accuracy of the results. It is very important, therefore, that the slits extend well out into the wings of the beam so that the true behavior of $\alpha(x)$ and $\sigma(x)$ in the wings is known.

Note that for $\Delta\theta > 0.5$ radians measured emittance is increasingly higher than predicted. Eq. (11), used to calculated the emittance added to the beam by scattering in a titanium foil, becomes increasingly invalid at higher scattering angles. This would explain the behavior of the total effective emittance curve shown in Fig. 10. For large scattering angles the assumptions used in deriving Eq. (11) break down (the foil begins to approach a significant percentage of range thickness) and scattering angles increase dramatically with increasing foil thickness. This is precisely the behavior observed in Fig. 10.

VII. CONCLUSION

The emittance diagnostic shows promise as a method of accurately measuring the emittance of a pulsed electron beam. Emittance measurements yield reasonable values of emittance when using thin foils. For the thicker foils our formula for estimating the emittance breaks down. Table 3.6 shows the values of emittance averaged over the shots taken using 2.5 mils thick Titanium before the mask. Here the emittance is normalized by π to allow comparison with ε_{eff}.

	Estimated ε	**Measured** ε
ε_{eff}	6.31	11.92
$\varepsilon_{63\%}$	8.96	4.59
$\varepsilon_{90\%}$	13.00	9.88

Table 3 Average measured emittance values found when using 2.5 mils of Titanium foil (using $\varepsilon = A_X/\pi$).

The ultimate calibration of the emittance diagnostic relies on theory. Attempts to assess the accuracy of this device by creating beams of varying emittance are met with limited success. The time integrated nature of the data complicates the analysis as does the breakdown of Eq. (11) when using the thicker foils. An accurate method of providing a beam of known emittance is required to validate the device. This may be

ranging from 1.5 to 3 mils. Eq. (11) could still be used to estimate emittance if we restrict the study to low values of $\Delta\theta$. These shots should be time resolved to simplify interpretation of the emittance ellipse.

There are several improvements to the device and analysis techniques that could be incorporated into the next generation diagnostic to improve the accuracy and reliability of the measurements.

For intense, low emittance beams, space charge expansion of the beamlets within the emittance meter can cause a small but significant increase in measured emittance. Keeping the Cherenkov foil as close to the slit as possible will help to mitigate this effect. Provisions could be made in the analysis to compensate for the expansion using Eq. (3).

A study of the effects of focusing and exposure for a beam of known emittance should be done to determine how critical these parameters are. Effort should be made to use as small an f-stop as possible when photographing the Cherenkov foil in order to relax the focusing requirements. Using film of wider dynamic range would relax the exposure requirements.

A new mask should be constructed with longer slits covering a wider area. This would place slits well out into the wings of the beam and dramatically improve the accuracy of the reconstructed beam parameters $\alpha(x)$ and $\beta(x)$. A greater number of slits would increase the number of data points available for the beam parameters allowing for a better curve fit and a more accurate determination of beam centering and axisymmetry. It would also allow for a more detailed construction of the emittance ellipse. This is important if one wishes to observe distortion or filamentation in the ellipse. Longer slits would allow a fit to be performed lengthwise to determine beam centering and to verify the curve for $\beta(x)$.

VIII. ACKNOWLEDGMENTS

We would like to thank Dr. Robert Pechacek for valuable assistance in perfecting the optical data collection system, and to Matt Myers for assistance in running the Pulsrad and Super-Ibex accelerators. Thanks also go to Bill Dolinger and Gary Littlejohn for assistance in running the accelerators and for machining parts used in this experiment. This work was supported by the Office of Naval Research.

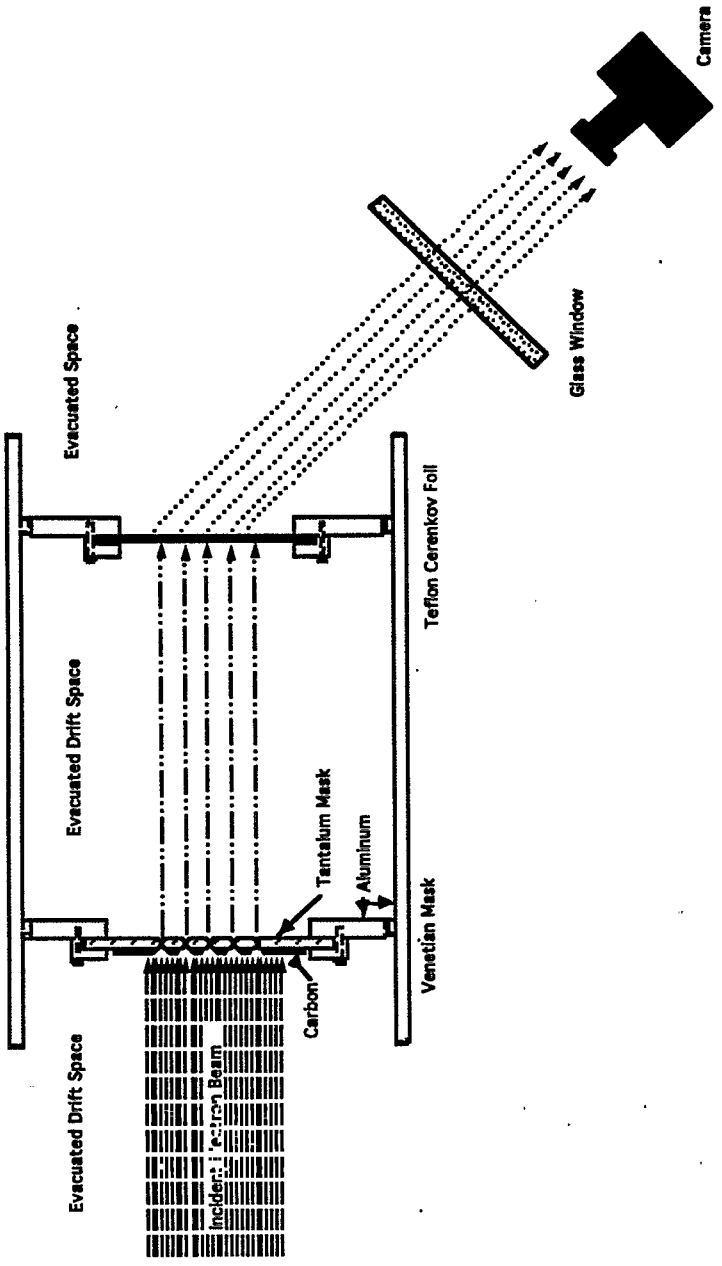

Figure 1 Schematic diagram of emittance diagnostic.

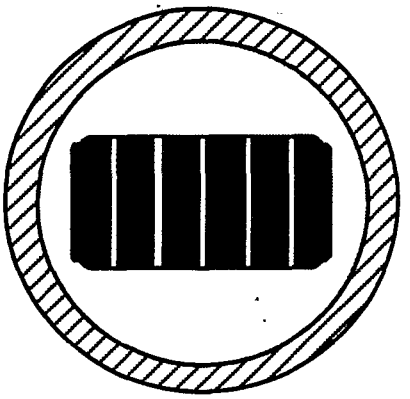

Figure 2 Venetian blind mask (beam incident into page).

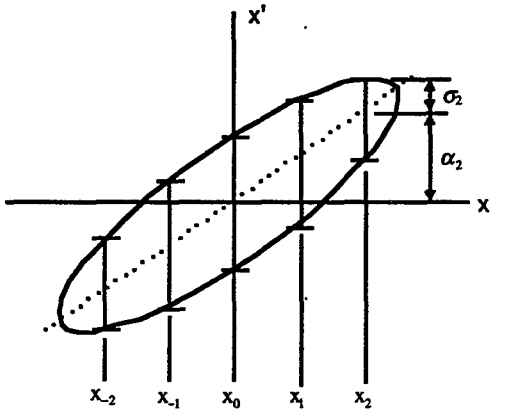

(a)

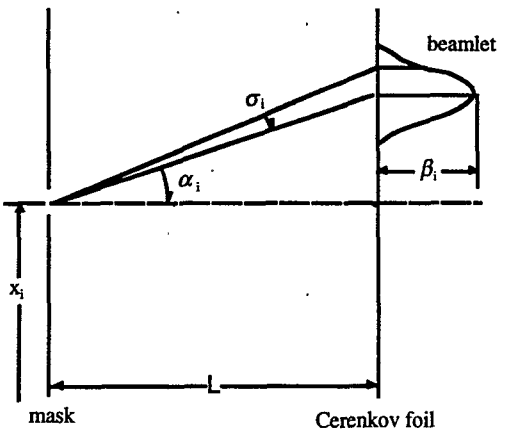

(b)

Figure 3 Construction of the emittance ellipse.

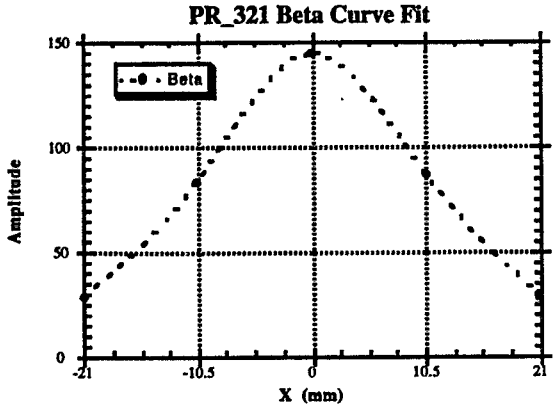

(a)

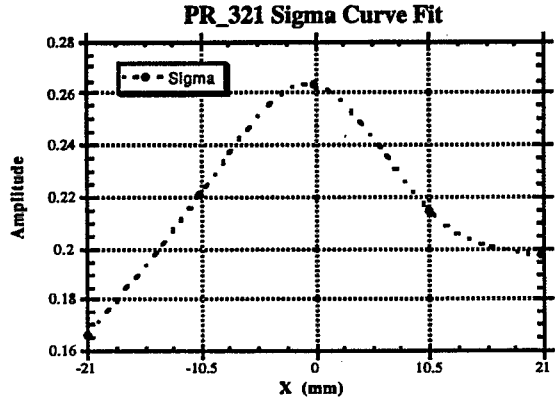

(b)

Figure 4 Parameter plots of $\beta(x)$ and $\sigma(x)$ for PR_321.

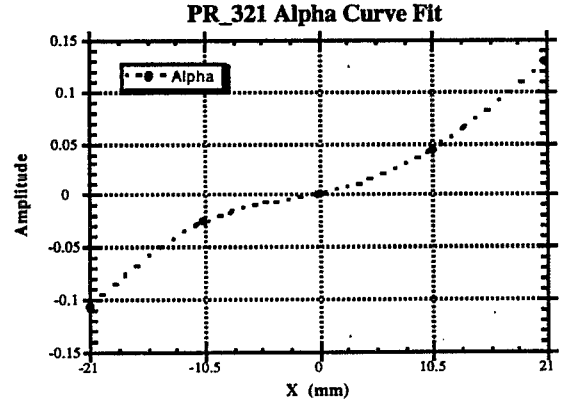

Figure 5 Parameter plot of $\alpha(x)$ for PR_321.

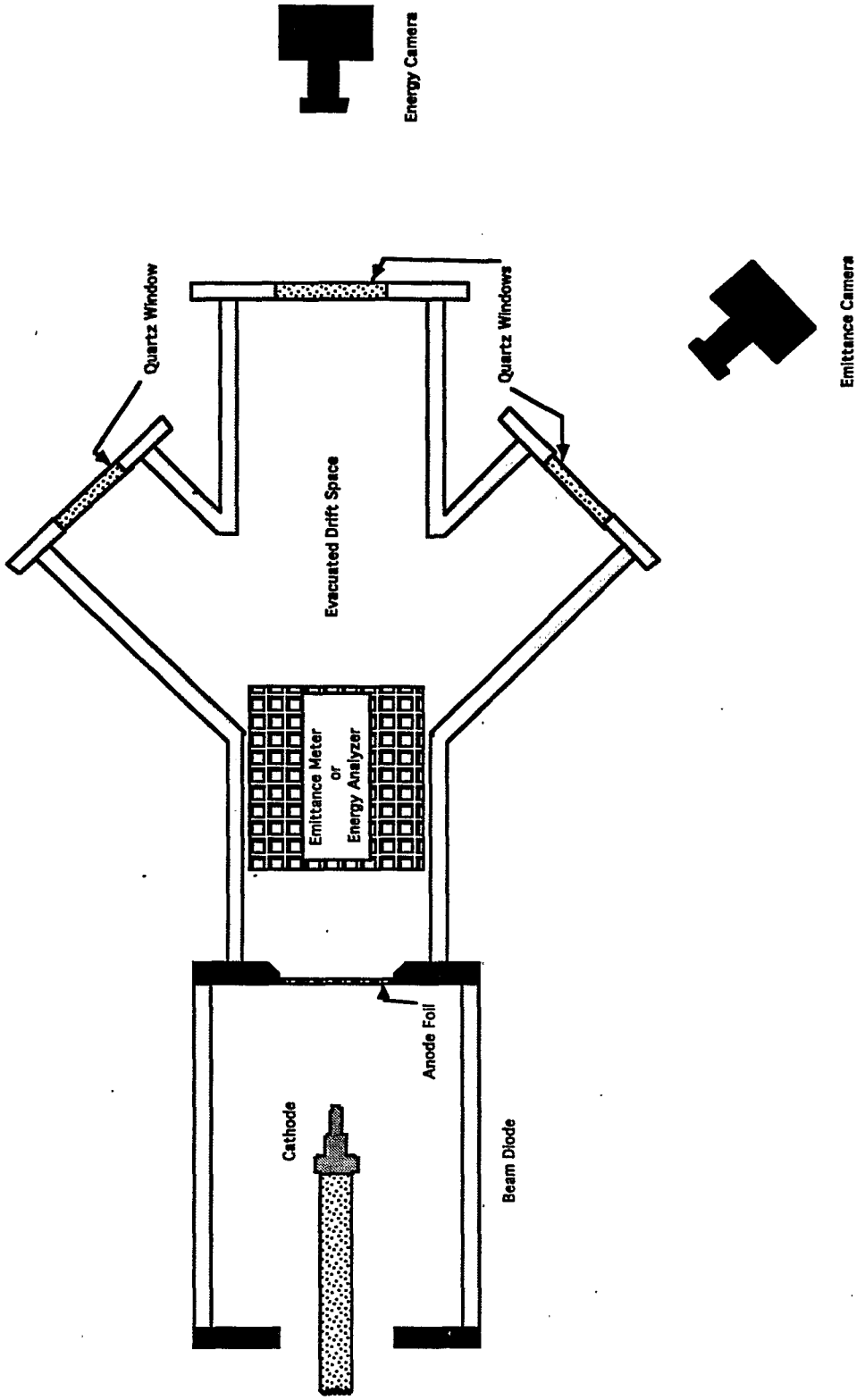

Figure 6 Beam diode and typical experimental setup.

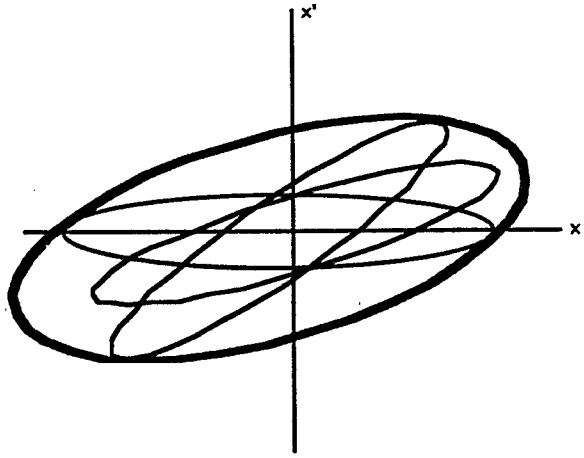

Figure 7 Effect of time integration on emittance measurement.

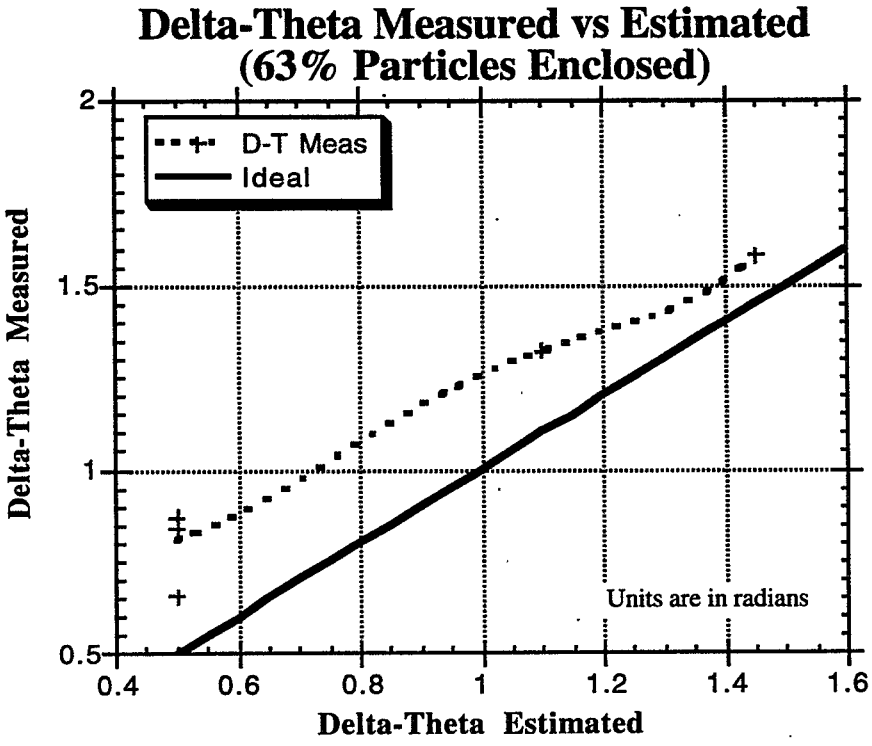

Figure 8 Measured vs estimated $\Delta\theta$ for %P = 63%.

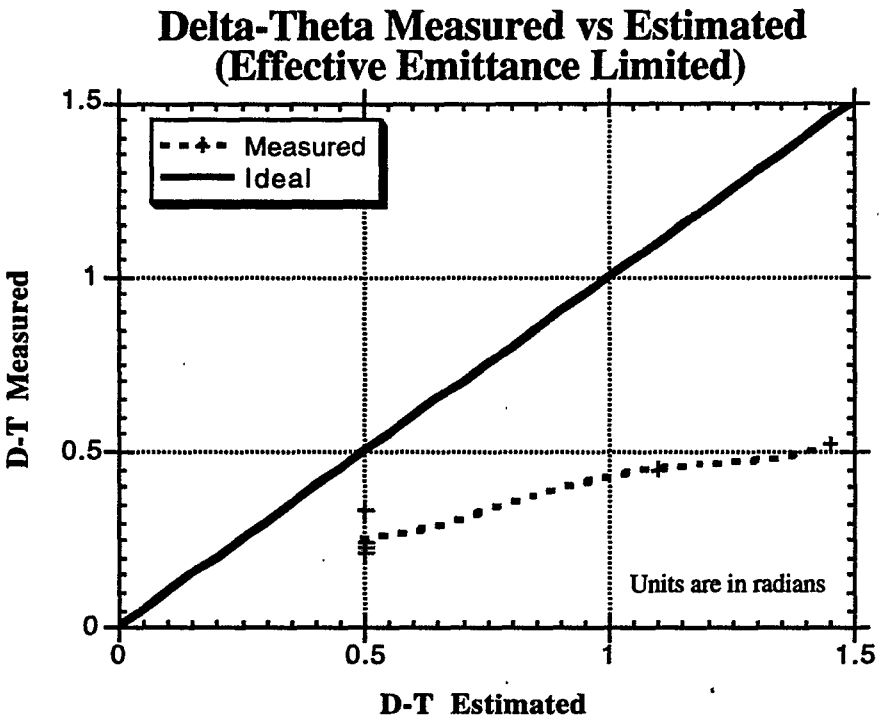

Figure 9 Measured vs estimated $\Delta\theta$ for ε_{eff} limited.

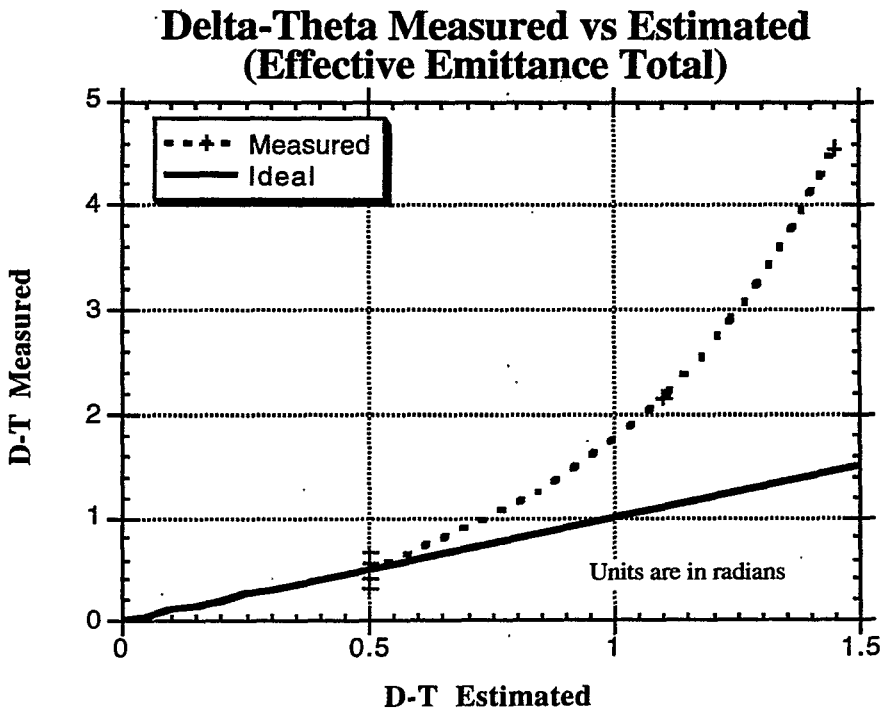

Figure 10 Measured vs estimated $\Delta\theta$ for ε_{eff} total.

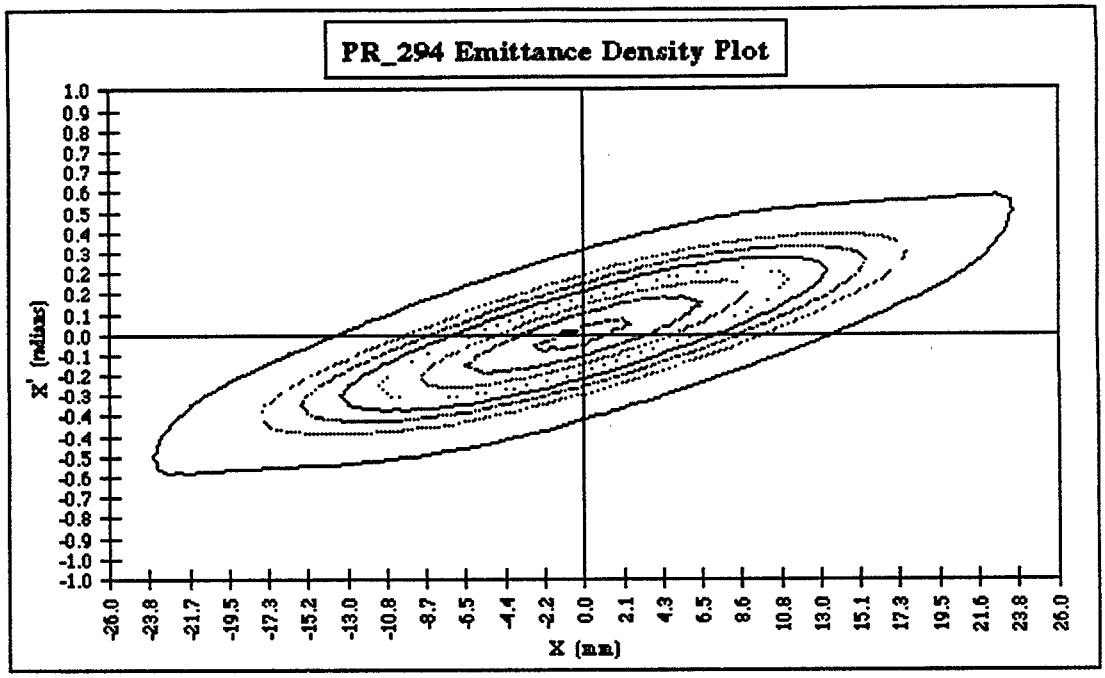

Figure 11 2-D phase space density plot of PR_294.

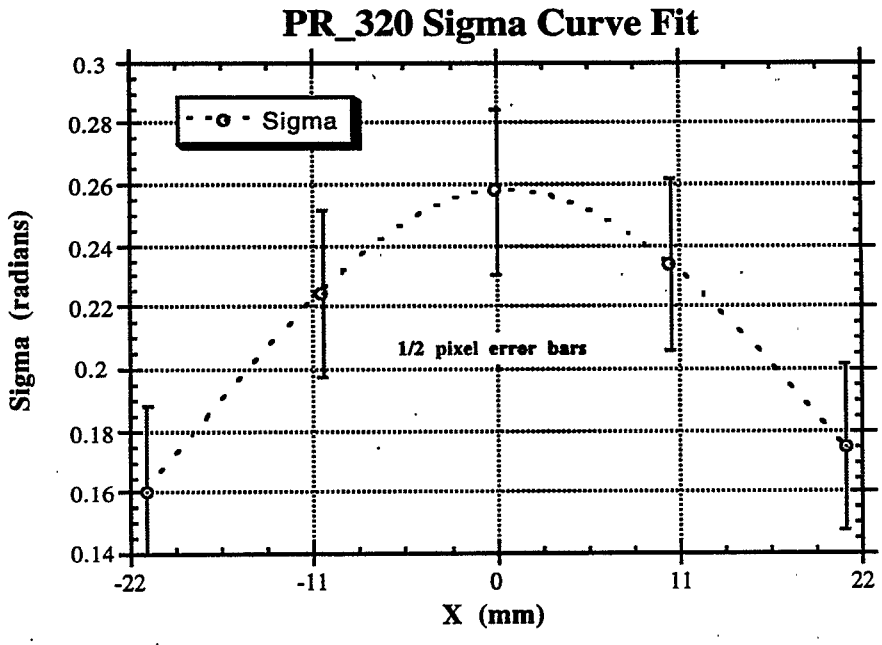

Figure 12 Cubic spline fit to $\sigma(x)$ with error bars.

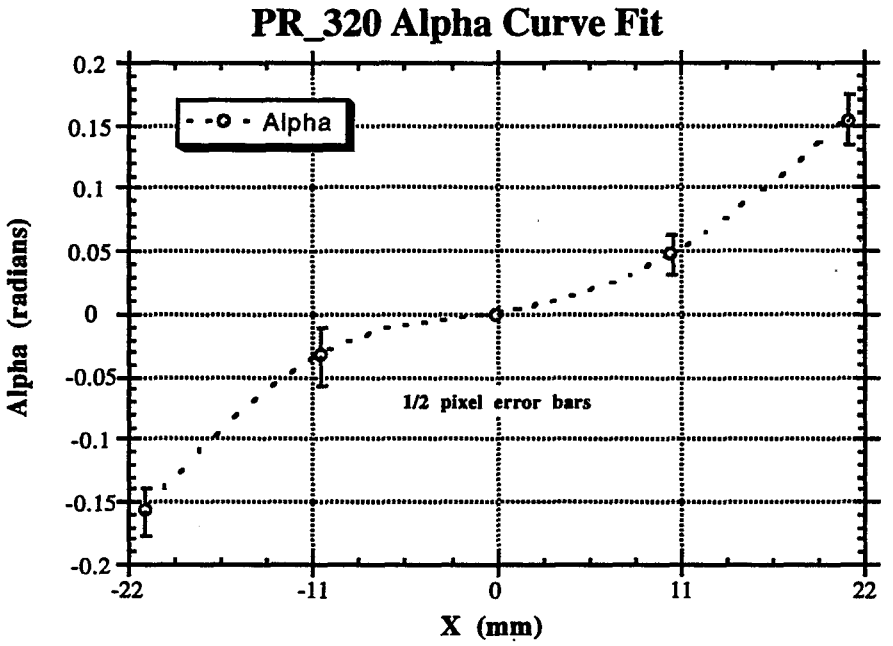

Figure 13 Cubic spline fit to $\alpha(x)$ with error bars.

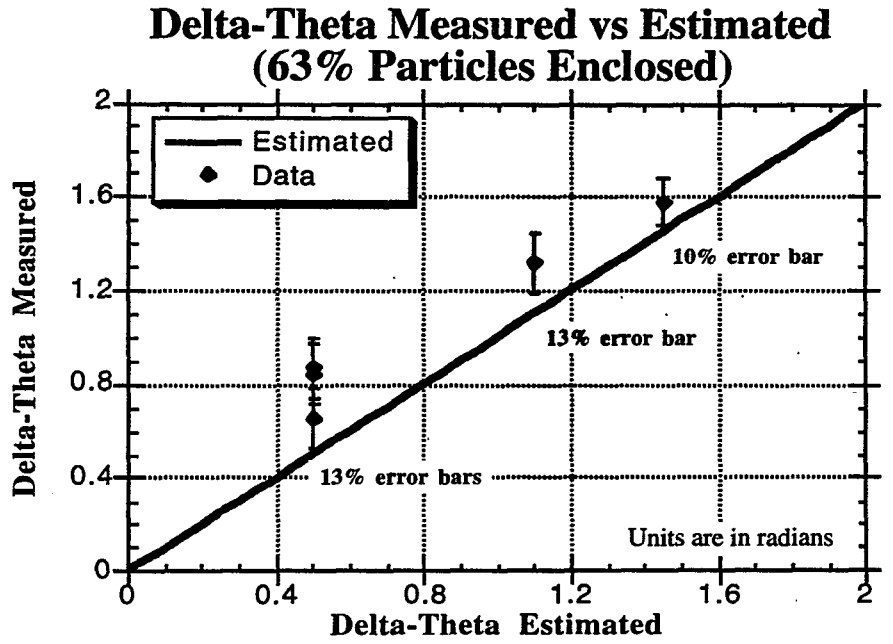

Figure 14 $\Delta\theta$ measured vs estimated with error bars.

VIII. REFERENCES

1. C. Lejeune and J. Aubert, in Applied Charged Particle Optics, edited by A. Septier (Academic, New York, 1980), pp. 159-259.

2. Series 300 Pulserad Specifications, Data sheet.

3. "Status of Emittance Measurements", Internal paper, CPB, 1987.

4. T.A. Peyser, J. A. Antoniades, M. C. Meyers, M. Lampe, R. E. Pechacek, D. P. Murphy, R. A. Meger, "A segmented concentric faraday cup for measurement of time dependent relativistic electron beam profiles", Rev. Sci. Instrum. 62, 2895, (1991).

5. M. Reiser, Theory and Design of Charged Particle Beams, Manuscript, 1991.

6. M. J. Rhee and K. A. Boulais, "Root-mean-square emittance of multiple beam systems", Phys. Fluids B **3** (7), 1781-1786, (1991).

7. R. A. Meger, "Non-neutral beam expansion due to space charge and emittance", CPB tech-note no. 89-4, 1989.

8. M. J. Rhee and R. F. Schneider, "Phase-space measurements of a beam with a Maxwellian transverse velocity distribution by a finite-width slit", Rev. Sci. Instrum. 62 (6), 1468-1470, (1991)

9. Commercial spreadsheet software, Claris Resolve v1.0, (Claris Corp., 1991).

10. M. J. Rhee and R. F. Schneider, "The root mean square emittance of an axisymmetric beam with a Maxwellian velocity distribution", Particle Accelerators, 20, 133-141, (1986)

11. C. Ekdahl, (private communication).

12. W. Namkung and E. P. Chojnacki, "Emittance measurements of space-charge-dominated electron beams", Rev. Sci. Instrum. 57 (3), 341-345, (1986).

13. R. B. Miller, An Introduction to the Physics of Intense Charged Particle Beams (Plenum Press, New York, 1982).

14. M. J. Rhee, "Refined definition of the Beam Brightness", University of Maryland Laboratory for Plasma Research, to be published in Phys. Fluids in 1992.

15. J. D. Lawson, The Physics of Charged-Particle Beams (Clarendon Press, Oxford Science Publications, 1988).

16. S. Humphries, Jr., Charged Particle Beams (John Wiley & Sons, New York, 1990).

17. H. Goldstein, Classical Mechanics (Addison-Wesley, 1981).

18. M. Reiser, G. Schmidt, "Relativistic Beam Relationships", CPB Report #91-015, University of Maryland Laboratory for Plasma Research, 1991.